

Overview of sun photometer measurements of aerosol properties in Scandinavia and Svalbard

C. Toledano^{a,*}, V.E. Cachorro^a, M. Gausa^b, K. Stebel^c, V. Aaltonen^d, A. Berjón^a, J.P. Ortiz de Galisteo^a, A.M. de Frutos^a, Y. Bennouna^a, S. Blindheim^b, C.L. Myhre^c, G. Zibordi^e, C. Wehrli^f, S. Kratzer^g, B. Hakansson^h, T. Carlund^h, G. de Leeuw^{d,i,j}, A. Herber^k, B. Torres^a

^a Grupo de Optica Atmosferica, Universidad de Valladolid, Valladolid, Spain

^b Andøya Rocket Range, Andenes, Norway

^c Norwegian Institute for Air Research, Kjeller, Norway

^d Finnish Meteorological Institute, Climate Change Unit, Helsinki, Finland

^e Joint Research Centre, Ispra, Italy

^f World Radiation Center, Davos, Switzerland

^g Stockholm University, Stockholm, Sweden

^h Swedish Meteorological & Hydrological Institute, Sweden

ⁱ University of Helsinki, Department of Physics, Helsinki, Finland

^j TNO Built Environment and Geosciences, Utrecht, The Netherlands

^k Alfred-Wegener-Institut für Polar- und Marine Research (AWI), Bremerhaven, Germany

ARTICLE INFO

Article history:

Received 8 April 2011

Received in revised form

26 September 2011

Accepted 11 October 2011

Keywords:

Aerosol
Sun photometer
Arctic
Scandinavia

ABSTRACT

An overview on the data of columnar aerosol properties measured in Northern Europe is provided. Apart from the necessary data gathered in the Arctic, the knowledge of the aerosol loading in nearby areas (e.g. sub-Arctic) is of maximum interest to achieve a correct analysis of the Arctic aerosols and transport patterns. This work evaluates data from operational sites with sun photometer measurements belonging either to national or international networks (AERONET, GAW-PFR) and programs conducted in Scandinavia and Svalbard. We enumerate a list of sites, measurement type and periods together with observed aerosol properties. An evaluation and analysis of aerosol data was carried out with a review of previous results as well. Aerosol optical depth (AOD) and Ångström exponent (AE) are the current parameters with sufficient long-term records for a first evaluation of aerosol properties. AOD (500 nm) ranges from 0.08 to 0.10 in Arctic and sub-Arctic sites (Ny-Ålesund: 0.09; Andenes: 0.10; Sodankylä: 0.08), and it is somewhat higher in more populated areas in Southern Scandinavia (AOD about 0.10–0.12 at 500 nm). On the Norwegian coast, aerosols show larger mean size (AE = 1.2 at Andenes) than in Finland, with continental climate (AE = 1.5 at Sodankylä). Columnar particle size distributions and related parameters derived from inversion of sun/sky radiances were also investigated. This work makes special emphasis in the joint and collaborative effort of the various groups from different countries involved in this study. Part of the measurements presented here were involved in the IPY projects Polar-AOD and POLARCAT.

© 2011 Elsevier Ltd. All rights reserved.

1. Introduction

The study of the atmospheric aerosols in the Arctic environment has strongly developed since the 1950s, when the first observations of haze were reported (Mitchell, 1956; Shaw, 1995). The Arctic has been shown to be a very sensitive area to climate change and the magnitude of the aerosol radiative forcing in polar regions is largely uncertain due to the spatial inhomogeneities, the variable surface

albedo and the solar geometry. In general, the quantification of the direct and indirect forcing by aerosols remains an outstanding problem (IPCC, 2007)(Solomon et al., 2007).

Despite the Arctic is almost free of anthropogenic aerosol sources, aerosol particles transported from mid-latitude regions can reach the Arctic and remain long time due to the reduced removal mechanisms, the high atmospheric stability and the low water content (Bodhaine and Dutton, 1993; Shaw, 1995). A review about this phenomenon, the so-called Arctic haze, can be found in Quinn et al. (2007). Several authors have reported the long-range transport of aerosols of different origin into the Arctic, e.g. biomass burning aerosols from boreal regions (Stohl et al., 2006;

* Corresponding author. Tel.: +34 983423270; fax: +34 983423013.
E-mail address: toledano@goa.uva.es (C. Toledano).

Stone et al., 2008), from agricultural fires in Eastern Europe (Stohl et al., 2007; Treffeisen et al., 2007; Lund Myhre et al., 2007), Saharan dust (Rodriguez et al., 2008) or Asian pollution and dust (Di Pierro et al., 2011).

The aerosol observations in the Arctic are still scarce and not sufficient to resolve the large spatial variability. Experimental conditions, such as low temperatures and humidity, low solar elevation, high surface albedo and very low optical depth, make aerosol measurements difficult, especially passive remote sensing from ground and satellite, that allows routine aerosol monitoring at lower latitudes (Holben et al., 2001; Remer et al., 2008).

In order to improve the aerosol monitoring at high latitudes, ground-based aerosol networks have established routine observations in the Arctic, i.e. the Global Atmospheric Watch (GAW), the Co-operative Programme for Monitoring and Evaluation of the Long-range Transmissions of Air Pollutants in Europe (EMEP) and Aerosol Robotic Network (AERONET). The number of operational sites notably increased with the stimulus of the International Polar Year 2007–2008 (www.ipy.org). Several projects within the IPY frame, like Polar-AOD (Mazzola et al., *in press*) and POLARCAT, promoted this kind of long-term aerosol observations. Aside from these networks, some institutions have maintained long-term sites for aerosol monitoring, as it is the case of Barrow (U.S), Alert (Canada) and Ny-Ålesund (Svalbard). At these sites, very valuable databases allowed the analysis of trends in the aerosol load and composition (Sirois and Barrie, 1999; Quinn et al., 2007; 2009).

This paper is focused on the aerosol observations with sun photometers. Global sun photometer networks like GAW-PFR (Wehrli, 2005) and AERONET (Holben et al., 1998), (including the subnetworks AEROCAN and RIMA), maintain sites in the North American and European Arctic sectors. These networks impose standardization of instruments, processing and calibration, as well as traceability to calibration references.

The columnar optical and microphysical properties obtained with these instruments allow characterizing the aerosols (Bokoye et al., 2002; Aaltonen et al., 2006; Toledano et al., 2006; Rodríguez et al., *in press*; Zdun et al., 2011). However sun photometer data series are still short for the AERONET and GAW sites, compared to the long datasets available at Ny-Ålesund (Herber et al., 2002) or Barrow (Polissar et al., 1999), and other sites further south like Norrköping

(Sweden). In principle, optical properties from sun photometer allow the estimation of the aerosol direct radiative forcing (Haywood and Boucher, 2000; Myhre et al., 2003; 2007), but it must be noted that information on the absorption properties (i.e. single scattering albedo) is difficult to obtain with sufficient accuracy when the aerosol load is low, namely AOD (440 nm) < 0.4 (Dubovik et al., 2000). A review on aerosol optical depth in the polar regions was given by Tomasi et al. (2007), in this case combined with in situ observations that are out of the scope of our study.

The aim of this paper is to provide an overview on the data of columnar aerosol properties measured in Northern Europe and their spatial and seasonal characteristics. Apart from the necessary data gathered in the Arctic, the knowledge of the aerosol loading in nearby areas (e.g. sub-Arctic) is of maximum interest to achieve a correct analysis of Arctic aerosols and transport patterns, the north-south gradients as well as the transformations of the aerosol on its way to the high Arctic. This work evaluates the data from operational sites with sun photometer measurements belonging either to national or international networks and programs conducted in Scandinavia and Svalbard (Spitsbergen). We will first describe the sites and instrumentation involved in this study, then the methodology applied for the determination of aerosol properties and afterward we provide summary of the results about the aerosol optical depth, the Ångström exponent and microphysical properties (size distributions), before presenting the conclusions.

2. Sites and instruments

2.1. Sites

The list of sites that were considered in this study is shown in Table 1 and on the map in Fig. 1. Most of them are associated to the above mentioned networks. Some of them have discontinued but still have long and valuable datasets.

We classified the sites in three groups: high Arctic (Svalbard); North of Scandinavia (sub-Arctic); and middle-southern Scandinavia. In the latter region, the number of sites increased considerably during the last decade (see Fig. 1). Midnight sun occurs above the Arctic circle (66.5°N). For instance, at Andenes (69°N) the

Table 1

List of sun photometer sites in the European Arctic sector and Scandinavia. List of institutions: Andoya Rocket Range (ARR); Alfred Wegener Institute for Polar and Marine Research (AWI); European Space Agency (ESA); Finnish Institute of Marine Research (FIMR); Finnish Meteorological Institute (FMI); Goddard Space Flight Center (GSFC); Joint Research Centre (JRC); Norwegian Institute for Air Research (NILU); Polish Academy of Science (PAN); Swedish Meteorological and Hydrological Institute (SMHI); Swedish National Space Board (SNSB); Stockholm University (SU); University of Valladolid (UVA); World Radiation Center (WRC).

Site	Institution	Coordinates	Network	Instrument	Start	End	N. months
Hornsund	GSFC,PAN	77.0°N, 15.6°E	AERONET	Cimel	2004	–	38
Longyearbyen	GSFC	78.2°N, 15.6°E	AERONET	Cimel	2003	2004	10
Ny_Ålesund	AWI	78.9°N, 11.9°E	Polar-AOD	SP1A	1991	–	114
Ny_Ålesund	NILU,WRC	78.9°N, 11.9°E	GAW-PFR	PFR	2002	–	50
Andenes	UVA,NILU,ARR	69.3°N, 16.0°E	AERONET-RIMA	Cimel	2002	–	46
Kiruna	SMHI	67.8°N, 20.4°E	GAW-PFR	PFR	2007	–	34
Sodankylä	FMI	67.4°N, 26.6°E	GAW-PFR	PFR	2004	–	48
Birkenes	NILU, UVA	58.4°N, 8.3°E	AERONET-RIMA	Cimel	2009	–	14
Gotland	SMHI	57.9°N, 19.0°E	AERONET	Cimel	1999	2004	34
Gustav_Dalen_Tower	JRC	58.6°N, 17.5°E	AERONET	Cimel	2005	–	34
Helsinki	FMI	60.2°N, 25.0°E	AERONET	Cimel	2008	–	20
Helsinki_Lighthouse	JRC, FIMR	59.9°N, 24.9°E	AERONET	Cimel	2006	–	30
Hyytiälä	FMI	61.8°N, 24.3°E	AERONET	Cimel	2008	–	25
Jokioinen	FMI	60.8°N, 23.5°E	GAW-PFR	PFR	2004	–	42
Kuopio	FMI	62.9°N, 27.6°E	AERONET	Cimel	2008	–	25
Norrköping_1995	SMHI	58.6°N, 16.2°E		SPM2000	1995	–	166
Norrköping	SMHI,ESA,SNSB	58.6°N, 16.2°E	GAW-PFR	PFR	2007	–	46
Palgrunden	ESA, SU, SNSB	58.8°N, 13.2°E	AERONET	Cimel	2008	–	16
SMHI ^a	SMHI	58.6°N, 16.2°E	AERONET	Cimel	2001	2006	22
Visby	SMHI	57.7°N, 18.4°E	GAW-PFR	PFR	2007	–	48

^a The Norrköping station was AERONET site under the name 'SMHI'.

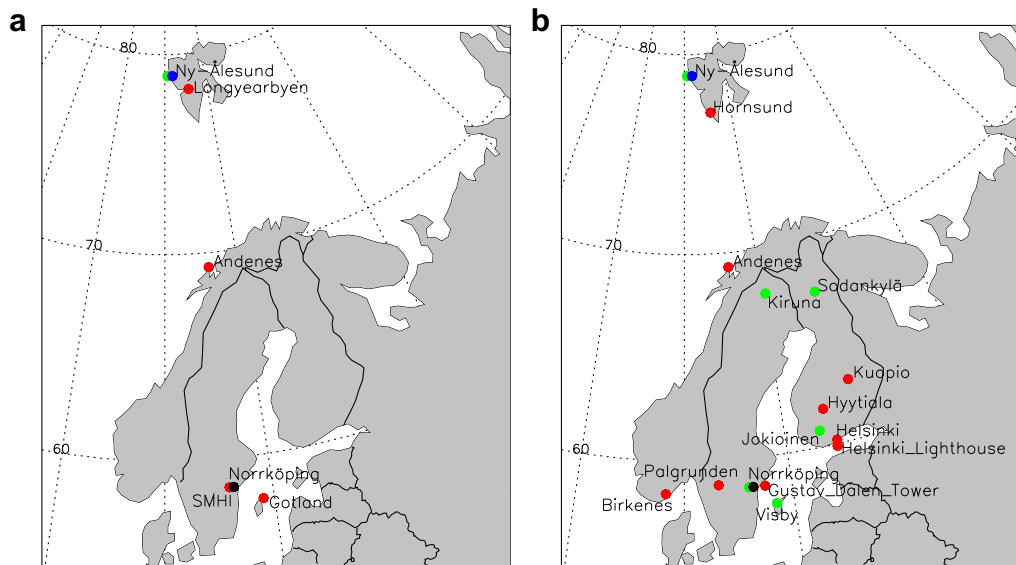


Fig. 1. Location of sun photometer sites in the European Arctic sector and Scandinavia: (a) Until 2003; (b) From 2004 on. Color symbols denote networks: AERONET sites (red), GAW-PFR (green), Polar-AOD (blue). (For interpretation of the references to colour in this figure legend, the reader is referred to the web version of this article.)

midnight sun period starts in the mid-May and lasts until mid-July. Conversely, the polar night spans from mid-November until late January. Both periods are longer further north. In Ny-Ålesund the polar night lasts from 26th October to 16th February.

Although southern Scandinavia is outside the Arctic circle, and sunphotometry is in principle possible during the entire winter, the maximum solar elevation in the winter months is in practice too low. In the AERONET quality-assured database (called level 2.0), no data at optical air mass larger than 5 are included (solar elevation 11.5°) and no measurements are collected when optical air mass at local noon exceeds 7.5 (solar elevation of 7.5° approximately).

The long records available at Ny-Ålesund and Norrköping are noteworthy (20 and 15 years respectively) and allow deriving a robust climatology. Several sites have about 4–5 year datasets (Andenes, Jokioinen, Sodankylä, Visby) whereas up to 8 new sites were set up after 2007. Note the improved spatial coverage in the region, especially in southern Scandinavia, before (Fig. 1a) and after 2004 (Fig. 1b).

2.2. Instruments

The operational networks have standardized instruments. Their characteristics are summarized in this section. We will emphasize their similarities and differences, that ultimately arise from the different aims and philosophy of the networks. Table 2 provides a summary of the main instrument characteristics.

The Cimel-318 is the standard instrument of AERONET. It is an automatic filter radiometer with 2-axis robot and 9 channels covering the spectral range 340–1020 nm (some models also have a 1640 nm channel). It collects direct sun measurements at these

Table 2
Summary of sun photometer characteristics.

Instrument	PFR	Cimel	SP1A	SPM2000
Spectral range	368–862 nm	340–1640 nm	350–1065 nm	368–778 nm
N. channels	4	9	17	3
Sun	1 min	5–15 min	1 min	1 min
Sky radiance	no	1 h (angular)	no	no
Temp. stabilized	yes	no	no	yes
AOD uncertainty	0.01	0.01–0.02	0.01	0.01–0.02

wavelengths, and sky radiances at four channels (or six for instruments with 1640 nm), i.e. 440, 670, 870 and 1020 nm in the almucantar and principal plane configurations. Direct sun measurements are performed every 15 min (more frequently at sunrise and sunset) to derive the aerosol optical depth and water vapor content, and sky radiances are measured every hour. Three direct sun measurements are performed within each measurement (triplet) in order to facilitate cloud screening. The Cimel is not thermostatted but a temperature sensor is located near the detector to provide temperature correction for the 1020 nm channel. A full instrument description is provided by Holben et al. (1998).

The Precision Filter Radiometer (PFR) is the instrument used in the GAW-PFR network. It acquires direct solar radiation at 4 spectral channels between 368 and 862 nm and it is designed for continuous and automated operation under a broad range of weather conditions. It has a thermostatic system that maintains the detector at $20.5 \pm 0.1^\circ\text{C}$ over an ambient temperature range from -20°C to $+35^\circ\text{C}$. This system eliminates the need for temperature corrections and prevents accelerated aging of filters. It requires an external solar tracker. A sensor in the PFR monitors the pointing quality for each measurement (Wehrli, 2005).

Since 1991, aerosol measurements have been performed at Ny-Ålesund by the Alfred Wegener Institute (AWI). Several instruments were used for this purpose, including Sun, Moon and Star photometers. The AOD at Ny-Ålesund during daylight conditions was measured using a sun photometer type SP1A produced by Dr. Schulz and Partner GmbH (<http://www.drschulz.com/cnt/>). It has a field of view of 1° and covers a spectral range from 350 nm to 1050 nm in 17 channels. The measured signal is temperature corrected and the operation temperature ranges from -30°C to $+40^\circ\text{C}$. The system is weather proof and an automatic sun tracking system guarantees continuous solar monitoring. Further details are provided by Herber et al. (2002). The sun photometer is yearly calibrated in high mountain sites, like the Izaña Observatory (Tenerife, Spain).

The SPM2000 sun photometer is an instrument manufactured by Centre Suisse d'Electronique et de Microtechnique (CSEM), Switzerland. It is a thermostatted 3-channel instrument for continuous direct sun measurements. The model used in Norrköping has the wavelengths 368, 500 and 778 nm. All channels are sampled every

3–6 s from which 1-min means are calculated, stored and then used for the AOD calculations. Its calibrations are traceable to PMOD/WRC (Physikalisch-Meteorologisches Observatorium Davos/World Radiation Center) reference instruments. A detailed description of the SPM2000 is given by Schmid and Wehrli (1995).

3. Method

For sun photometers collecting direct sun measurements, the aerosol optical depth at each spectral channel is derived from the Beer-Bouguer-Lambert law. This equation allows determining of the total optical depth of the atmosphere (τ)

$$F(\lambda) = F_0(\lambda) \cdot e^{-(\tau \cdot m)} \quad (1)$$

where $F(\lambda)$ is the direct sun signal at ground level at wavelength λ , $F_0(\lambda)$ is the extraterrestrial signal of the instrument, corrected by the Earth–Sun distance and m is the optical air mass in the measurement path (Kasten and Young, 1989).

The GAW-PRF and AERONET operational algorithms, separate the contributions of the molecules (R), aerosols (a) and absorbing gases (g) due to their different optical air masses at low solar elevation, which is an important aspect especially at high latitude sites:

$$F(\lambda) = F_0(\lambda) \cdot e^{-(\tau_R \cdot m_R + \tau_a \cdot m_a + \tau_g \cdot m_g)} \quad (2)$$

Taking into account the Rayleigh optical thickness (τ_R) corrected by local pressure and the gaseous absorptions (τ_g), the aerosol optical depth (AOD or τ_a) is:

$$\tau_a = [\text{Ln}(F_0(\lambda)/F(\lambda)) - \tau_R \cdot m_R - \tau_g \cdot m_g] / m_a \quad (3)$$

The channels used for aerosol investigation are located in spectral regions with weak absorption by atmospheric gases. To account for small absorptions by ozone, NO_2 , etc., effective absorption coefficients for each channel are calculated using the filter transmission curves. Amounts of these species were obtained from different sources: satellites (e.g. OMI), co-located ground-based measurements (e.g. Brewer) or monthly climatologies retrieved from measurements/models.

The Ångström exponent (AE), indicative of size predominance (Ångström, 1961), is obtained from the AOD at different wavelengths according to: $\tau_a(\lambda) = \beta \cdot (\lambda)^{-\alpha}$. Given the curvature of the AOD spectra, the Ångström exponent depends on the spectral range used in the retrieval. In AERONET this range is restricted to 440–870 nm. In the GAW-PFR the range for AE calculation is 368–862 nm.

Automatic cloud-screening algorithms are then applied to the data (Smimov et al., 2000; Alexandrov et al., 2004). These are based either on the temporal variability of the measured AOD, typically smaller than the variability of clouds, or the spectral signature of clouds, i.e. nearly wavelength independent optical depth.

The calibration constant for each channel is given by the extraterrestrial signal $F_0(\lambda)$. This value is determined by comparison with reference instruments, that are calibrated by the well-known Langley plot method (Shaw, 1983) at high altitude stations (Mauna Loa or Izaña). The instruments are typically calibrated before and after deployment to meet the network protocols.

Finally, the combined direct sun (AOD) and sky radiances can be inverted with different algorithms to retrieve a set of optical and microphysical aerosol properties: size distribution, refractive index,

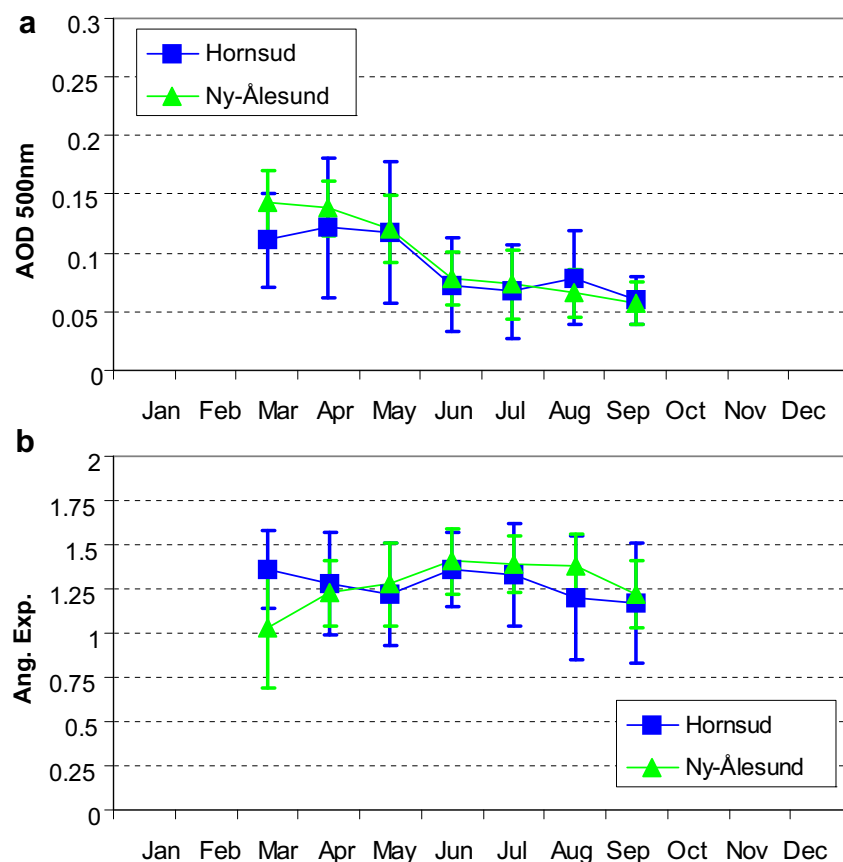


Fig. 2. Multi-annual monthly means of (a) aerosol optical depth (500 nm) and (b) Ångström exponent at the high Arctic sun photometer sites in Svalbard: Ny-Ålesund (2002–2010); Hornsund (2004–2010). Error bars give standard deviation.

phase function and single scattering albedo. This is the case for the AERONET data. The inversion algorithm by Dubovik and King (2000) is operationally applied to the almucantar radiances collected by the Cimel instruments. The uncertainty of the AERONET inversion products is described by Dubovik et al. (2000); (2006). These studies indicate that only for moderate turbidity conditions ($\text{AOD}(440\text{ nm}) < 0.4$) certain optical parameters, like the refractive index or single scattering albedo, can be retrieved with sufficient accuracy. This is not usually the case in Scandinavia, therefore the number of data of this kind is nearly insignificant and not suitable for a long-term characterization of such properties. We focused our study on the microphysical properties (size distributions and derived parameters), that can be adequately retrieved under all turbidity conditions.

For the AERONET sites, the level 2.0 database (cloud-screened and quality assured, for details see AERONET website) was used, both for the AOD and the inversion products. For the GAW-PFR and the other sites, cloud-screened and manually inspected data were utilized in the AOD analysis.

The accuracy achieved in the AOD measurement for each instrument is provided in Table 2. Despite the different concept and features of the instruments, the estimated AOD errors are similar and this fact may not introduce any bias in our analysis. Furthermore, the use of different retrieval algorithms (mainly regarding ancillary data: ozone, pressure, airmass) was analyzed within the POLAR-AOD project, and was shown not to produce significant differences in AOD calculations (about 0.005, i.e. within uncertainty) for a high Arctic site (Mazzola et al., in press). The POLAR-

AOD involved instruments from most of the sites included in this study and it also showed that most of the AOD differences among instruments arise from calibration errors and typically fall within the World Meteorological Organization recommendations (WMO, 2005). The specific calibration procedures in each network are well established and can be found in the corresponding publications (Holben et al., 1998; Wehrli, 2005; Herber et al., 2002).

4. Results and discussion

4.1. AOD and AE characterization

We have evaluated the multi-annual monthly means of aerosol optical depth and Ångström exponent for all sites listed in Table 1, although only the most representative (in terms of data amount and location) were considered in the discussion. The analysis of these magnitudes indicated differences in the seasonal patterns, which suggested the classification of the sites within three groups: Svalbard, northern Scandinavia and middle-southern Scandinavia.

The sites located in Svalbard, shown in Fig. 2 exhibit the known seasonal pattern in AOD, with maximum AOD in spring (about 0.12 at 500 nm wavelength), related to Arctic haze, and decrease in summer to very low values (about 0.06). According to the analysis of aerosol transport into the Arctic, Stohl (2006) demonstrated that the region north of 70°N is isolated from mid-latitude sources in summer, whereas in winter and spring the sources with larger potential impact are located in Eurasia (rather than North America or East Asia). During summer the aerosol removal processes are

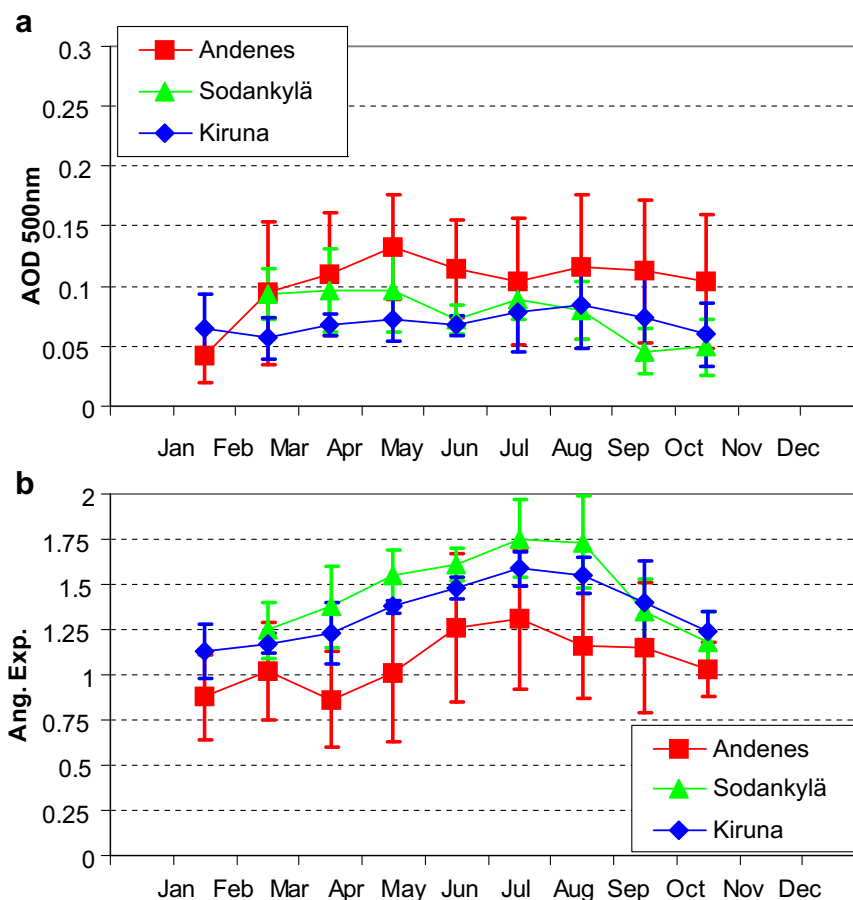


Fig. 3. Multi-annual monthly means of (a) aerosol optical depth (500 nm) and (b) Ångström exponent at the sites located in northern Scandinavia: Andenes (2002–2010); Kiruna (2007–2010); Sodankylä (2004–2010). Error bars give standard deviation.

more active in Svalbard. The Ny-Ålesund data shown in Fig. 2 belong to the GAW-PFR instrument, while Hornsund is an AERONET station. The results agree with the long-term means reported by the AWI station in Ny-Ålesund (Herber et al., 2002).

The AOD differences in March between Ny-Ålesund and Hornsund cannot be considered relevant due to the different temporal periods in each dataset. The year to year variability can be significant, especially when individual episodes have a large impact on observed monthly averages. That was the case for July 2004, when huge emissions from boreal forest fires in North America reached Svalbard (Stohl et al., 2006) and also in spring 2006, when agricultural fires in Eastern Europe resulted in elevated pollution levels in the Arctic (Stohl et al., 2007; Lund Myhre et al., 2007).

The Ångström exponent in Svalbard does not show as clear seasonal pattern as the AOD. Apparently there is a minimum in May at the end of the haze season, and then the AE increases slightly during the summer. In any case the multi-annual monthly means were above 1.0, thus indicating a fine particle predominance in general. The AE standard deviation in March (0.33) was almost 2 times larger than the rest of the months (0.18). In spring low values of AE were found during some months, showing persistent coarse particle predominance during certain periods that are related to the transport of Asian dust into the Arctic (Stone et al., 2007; Di Piero et al., 2011).

The next step was the analysis of the sites located in northern Scandinavia. The results are displayed in Fig. 3. The data amount is considerably less than in Svalbard, therefore these averages are subject to important changes as the databases grow in the following years. The AOD seasonal pattern is clearly different than

that of the Arctic sites. The values in March and April are low in general, with no signs of persistent haze in the monthly averages. Conversely, the AOD in summer does not decrease to very low values. The AOD was stable below 0.1 (at 500 nm) throughout the year at Sodankylä and Kiruna. Andenes exhibits slightly higher AODs. The maximum AOD in May for this site is related to certain individual episodes (Rodríguez et al., in press).

The three sites Andenes, Kiruna and Sodankylä are located at similar latitudes. However the site locations have important differences: The observatory in Andenes is located on the island Andøya at an altitude of 380 m a.s.l. Kiruna is located East of the Scandinavian mountain range and Sodankylä is further East in Finland, in a continental environment. The aerosol type was expected to be different and that was indicated by the Ångström exponents. The higher AE was found at the continental site Sodankylä, whereas the lower was found at the coastal site Andenes. This result is in agreement with the aerosol type characterization reported for key sites (Holben et al., 2001) dominated by continental and marine aerosols respectively.

Another important feature of the AE in northern Scandinavia is the similarity in the seasonal pattern, despite of site differences in aerosol background. The AE increased during spring and had a maximum in July for the three sites, followed by a decrease in autumn. Values ranged from 1 to 1.2 in March up to 1.3–1.75 in July. This seasonality would indicate the apportionment of fine particles in summer in this sub-Arctic region, although the origin or specific type cannot be derived from these data. Complementary aerosol measurements (in situ and chemical) may provide insight on this subject.

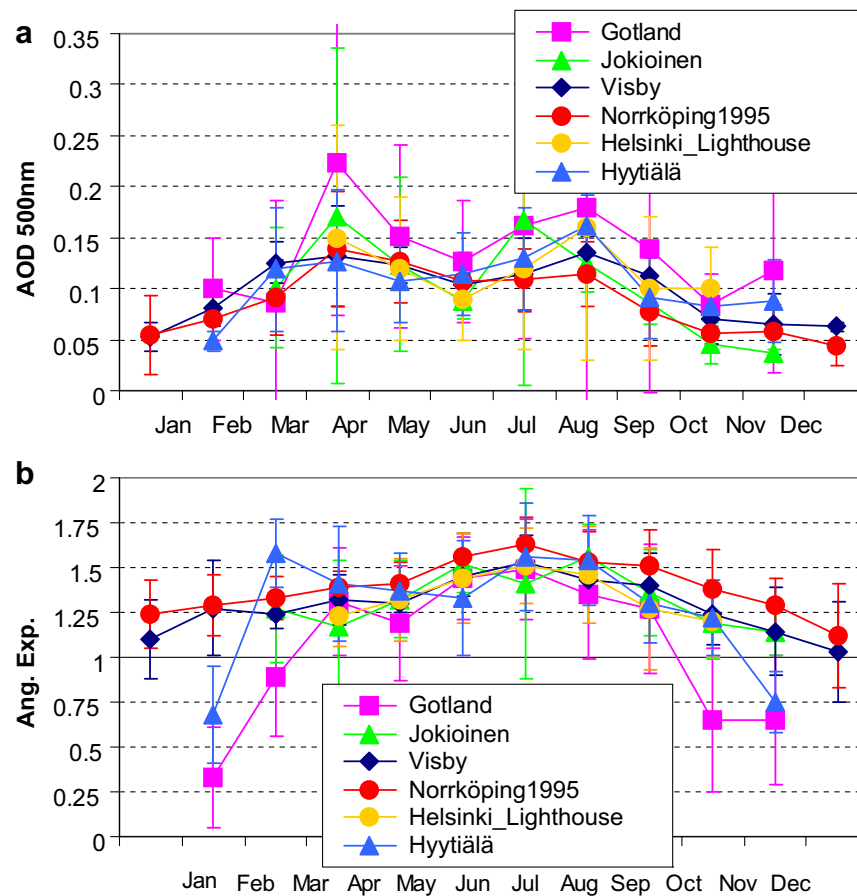


Fig. 4. Multi-annual monthly means of (a) aerosol optical depth (500 nm) and (b) Ångström exponent at the sites located in southern Scandinavia. The operation period for each site is listed in Table 1. Error bars give standard deviation.

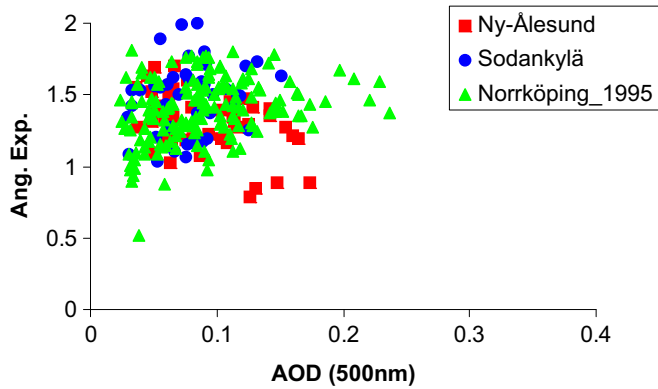


Fig. 5. Scatter plot of the Ångström exponent versus the aerosol optical depth (500 nm) monthly means at Ny-Ålesund (Svalbard), Sodankylä (Finland) and Norrköping (Sweden).

The AOD and AE for southern Scandinavia is shown in Fig. 4. Despite the variability of site locations, the AOD has a consistent seasonal pattern, which is, moreover, different from those in the high Arctic and the sub-Arctic sites. In southern Scandinavia the AOD peaks in April and August, with similar AOD (500 nm) about 0.15. Two minima in June (about 0.1) and December–January (about 0.05) are observed. The AOD maximum in April coincides with the snow melt and agricultural burning season in Eastern Europe (Stohl et al., 2007; Zdun et al., 2011), although rigorous transport pattern analysis would be required (in the fashion of Stohl, (2006)) to investigate the impact of this source (Korontzi et al., 2006). The second maximum in summer is observed in many European locations and is likely related to anthropogenic pollution, forest fires and drier weather conditions.

With the exception of Hyytiälä and Gotland during spring and autumn, the AE in the investigated sites Fig. 4b was rather similar for all sites. It showed minimum values in winter (about 1–1.2) and maximum in summer (about 1.5). These values indicate a clear fine

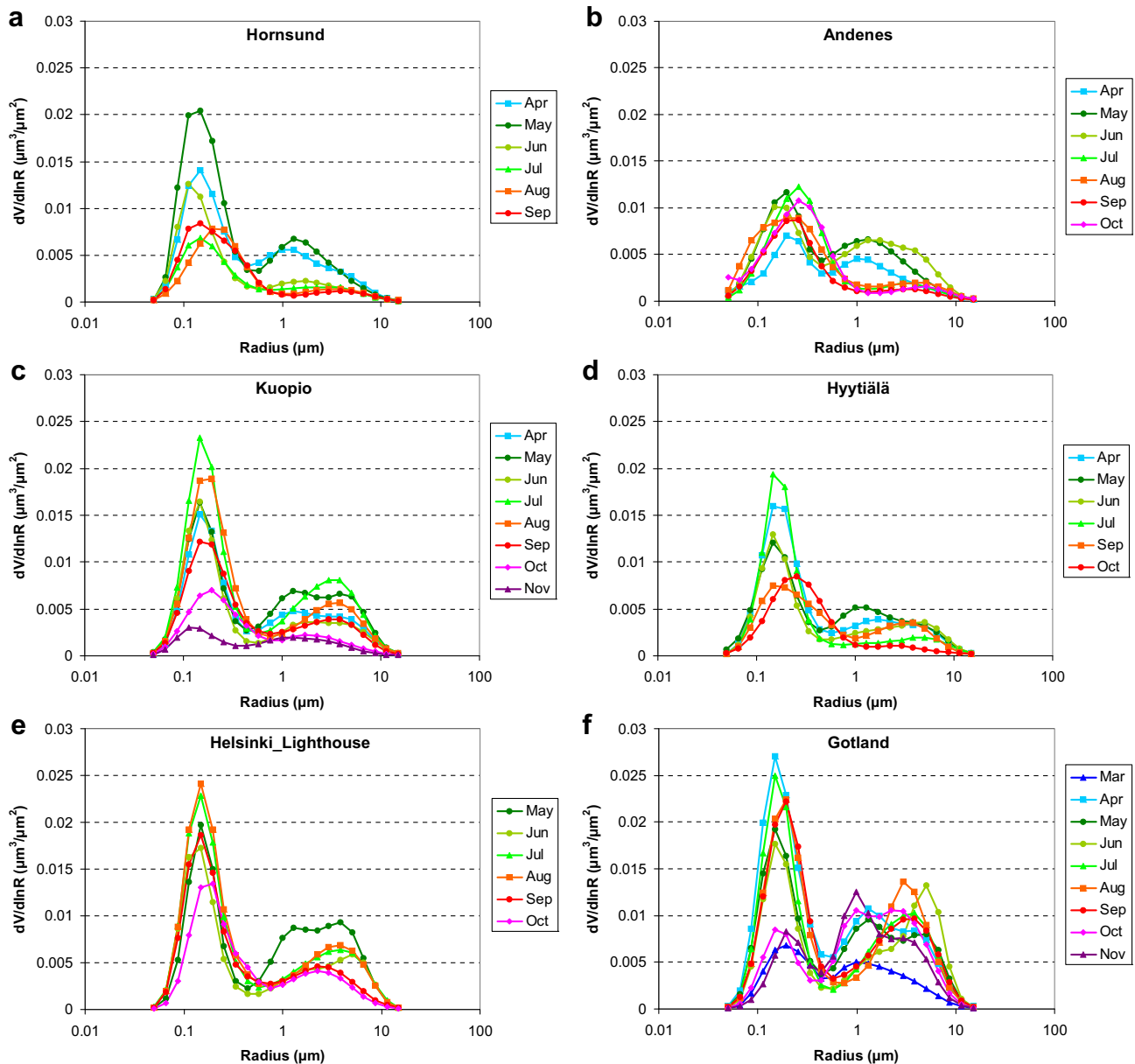


Fig. 6. Multi-annual monthly means of aerosol particle size distribution at 6 representative sites in Svalbard and Scandinavia. Note that winter months are missing for most of the sites.

particle predominance at all sites. The AE seasonality is somewhat independent from the AOD, although it may indicate smaller sizes during the summer AOD peak.

The AE vs. AOD scatter plot in Fig. 5 contains monthly means at 3 representative sites, in order to show the aerosol types that are relevant in the long-term analysis. The aerosol types are identified in this plot by comparison with climatological values at key sites (Holben et al., 2001). The spring months at Ny-Ålesund (red squares) exhibit AOD (500 nm) > 0.1 and AE between 0.8 and 1.5 (Arctic haze). The lowest AE values are associated to the presence of Asian dust, which is persistent enough to be significant in a monthly mean basis. The background summer values in Ny-Ålesund are in general characterized by low AOD (500 nm) below 0.08 and AE above 1.0. These values are very similar to those found during clean months in the sub-Arctic site Sodankylä and southern Scandinavia site Norrköping. In Sodankylä the aerosol type can be considered clean continental. All monthly means had AE above 1.0 and AOD (500 nm) below 0.15. The occurrence of higher AOD is episodic (up to few days) and is not relevant in longer time scales. Further south, in Norrköping, the

presence of polluted aerosols is observed, with monthly mean AOD (500 nm) above 0.15 and high associated AE above 1.3, which mostly corresponds to the AOD peak in spring, and also to some summer months. In winter the cleanest observations were obtained, with a wide range of AE (0.5–1.8), the higher values associated to clean continental aerosol and the lower to clean maritime aerosol.

4.2. Size distributions

The volume size distributions (level 2.0) for the AERONET sites have been investigated. Bear in mind that the strong retrieval restrictions and the reduced sampling of the sky radiances, make the number of these data very small. Note also the lack of data during winter. The multi-annual means for the available data at 6 representative sites are shown in Fig. 6.

These plots indicate a clear fine mode predominance in the volume size distributions for almost all sites and months. Only Gotland during autumn, where the maritime aerosols are obviously present, had coarse mode predominance. In general the volume

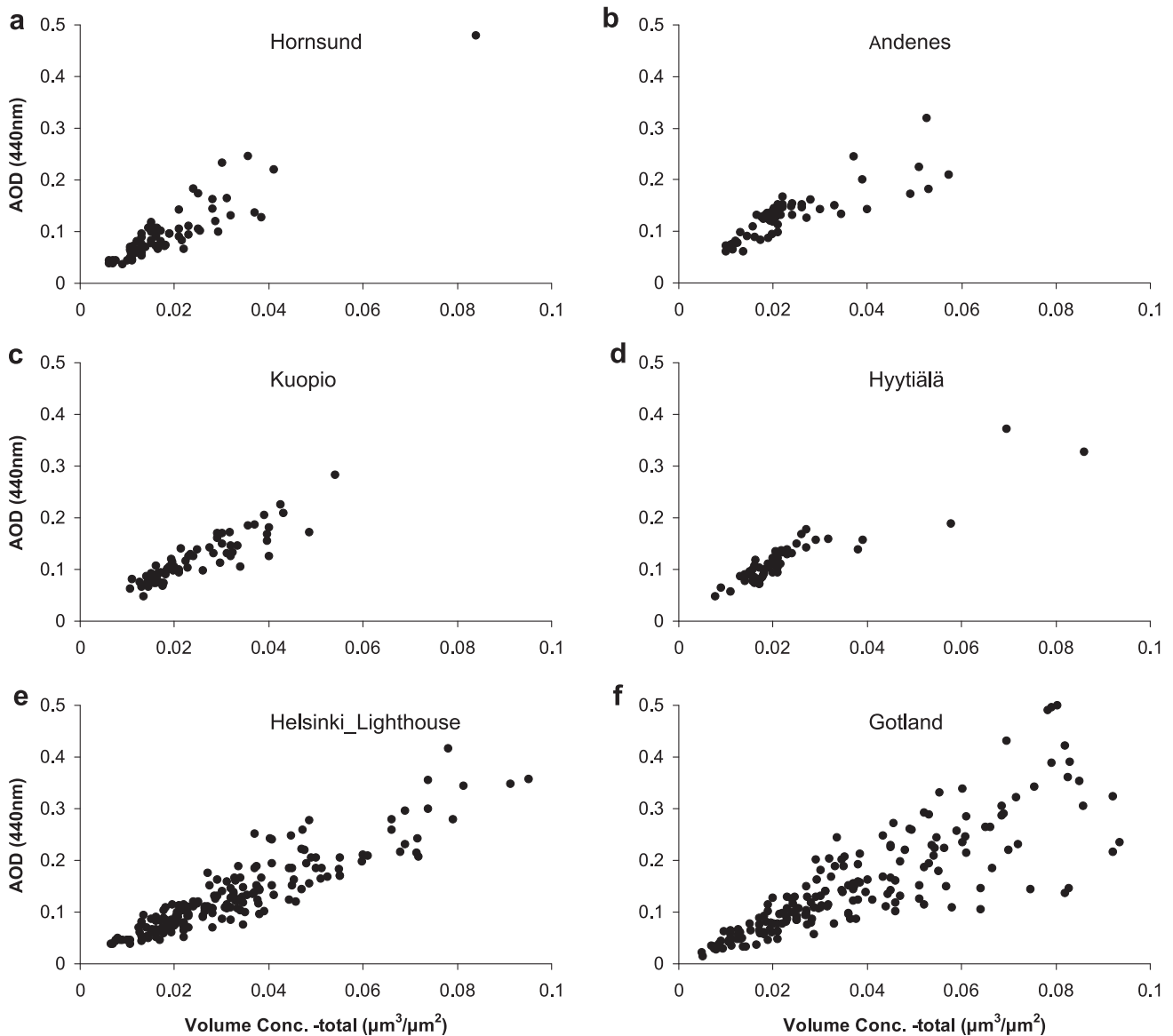


Fig. 7. Volume concentration ($\mu\text{m}^3/\mu\text{m}^2$) vs. Aerosol optical depth (440 nm) at 6 representative sites in Svalbard and Scandinavia. Data are Level 2.0 daily means.

Table 3

Summary of optical and microphysical properties for selected sites: aerosol optical depth (500 nm), Ångström exponent, volume concentration -total (V_t), fine mode fraction (V_f/V_t), columnar extinction coefficient (E_{col} (440nm)). N_{AOD} is the number of days with AOD data, whereas N_{inv} is the number of days with level 2.0 inversion data.

Site	AOD (500 nm)	AE	N_{AOD}	V_t [$\mu\text{m}^3/\mu\text{m}^2$]	V_f/V_t	E_{col} (440nm) [$\mu\text{m}^2/\mu\text{m}^3$]	N_{inv}
Hornsund	0.09	1.27	331	0.020	0.73	3.38	61
Andenes	0.10	1.18	368	0.019	0.69	4.25	58
Gotland	0.14	1.05	469	0.042	0.50	4.71	205
Helsinki_Lighthouse	0.12	1.35	452	0.035	0.64	3.60	188
Hyytiälä	0.11	1.27	267	0.023	0.66	3.76	53
Kuopio	0.10	1.39	230	0.026	0.70	3.37	71

concentrations were low. We found, however, some seasonal features that are described below.

At Hornsund (Svalbard), the fine mode concentration had a clear gradient, being higher in May and April, and lower during summer.

It is remarkable that the coarse mode almost disappeared in the summer months. In spring (haze season) both the fine and the coarse mode increased their concentrations, the largest increase corresponding to the fine mode.

The fine mode at Andenes (Norwegian sub-Arctic) is very stable throughout the year, in contrast with the high Arctic site described above. Furthermore, the lower fine mode concentrations are found in April and the autumn months. The coarse mode concentration decreases to very low values after June.

The southern site with more data and better coverage (March through November) is Gotland. At this site, the fine mode exhibits the highest mean concentrations, which are very stable from April to September. Only after October the fine mode decreases significantly, and the fine mode concentrations become even lower than those of the coarse mode. In these months the coarse particles of maritime origin are predominant in absence of fine mode particle apportioning. Actually the coarse mode is somewhat stable along the year and exhibits the highest average concentrations among all the investigated sites.

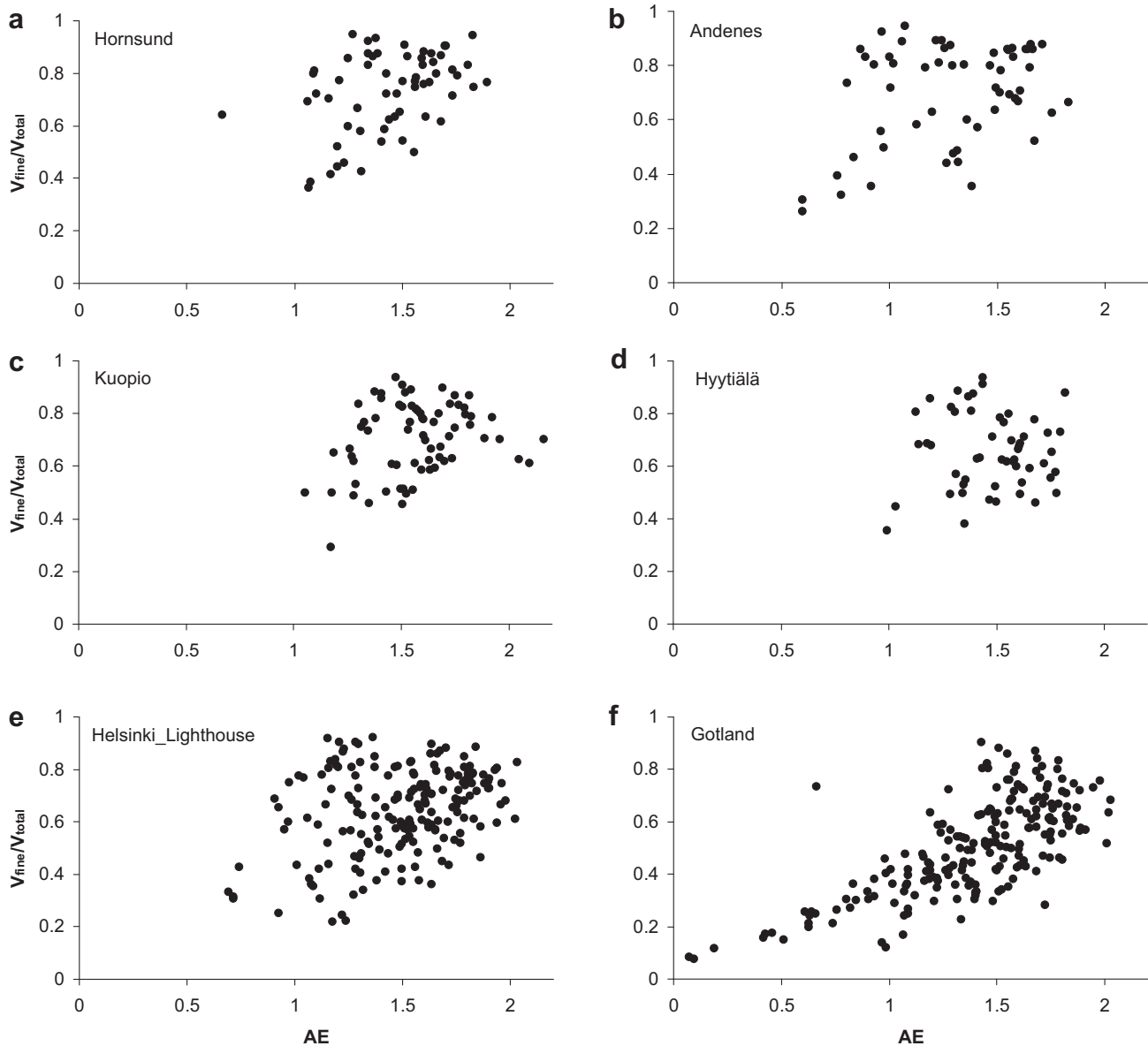


Fig. 8. Fine mode fraction of volume concentration (V_f/V_t) vs. Ångström exponent at 6 representative sites in Svalbard and Scandinavia. Data are Level 2.0 daily means.

The continental sites Kuopio and Hyytiälä are characterized by fine mode predominance, especially in July. The fine mode concentrations (and also the coarse mode) decrease in autumn. That is not the case for Helsinki, where the pollution from the city results in a higher background, thus the fine mode concentration does not diminish as much as at the other Finnish sites.

In order to further characterize the aerosol microphysics, we analyzed the volume concentrations for the total distribution (V_t), the fine mode (V_f) and the coarse mode (V_c), and the ratio of fine to total concentration (fine mode fraction, V_f/V_t), and relate them to the AOD and AE respectively. Furthermore, we derived the column extinction efficiency (similarly to mass extinction efficiency (Waggoner et al., 1981)), defined for the columnar magnitudes AOD and Volume concentration (Total), as: $E_{col}(\lambda) = AOD(\lambda)/V_t$. This parameter is closely related to the aerosol type.

The scatter plot of the AOD vs. total volume concentration (V_t) is shown in Fig. 7. The data are logically correlated and the slopes provide the columnar extinction efficiency. These values are provided in Table 3. This plot typically has two branches, the upper corresponding to fine particle dominated cases, and lower to coarse particles, since at 440 nm wavelength the fine particles have larger extinction efficiency. However the two branches are only clearly observable for Gotland site, Fig. 7f. Both fine and coarse particles were detected at this site, i.e. polluted/biomass burning aerosols and marine aerosols respectively. For this site, the extinction efficiency was the highest observed ($4.71 \mu\text{m}^2/\mu\text{m}^3$). At the other sites one main type is in general observed, dominated by fine particles, with extinction efficiencies in the range $3.3\text{--}4.2 \mu\text{m}^2/\mu\text{m}^3$.

Although the AE is a qualitative indicator of particle predominance (Schuster et al., 2006), the correlation of this parameter with the fine mode fraction derived from the volume size distributions is poor and requires careful analysis. The scatter plot of the AE vs. the fine mode fraction (V_f/V_t) is given in Fig. 8 for the same 6 representative sites. This kind of plot was shown for a large amount of AERONET data, covering all aerosol types, by Schuster et al. (2006). However few data with low AE are included there. The complete range of AE (including dust and marine aerosol) was shown by Prats et al. (in press) for a Spanish site. These papers indicate that the AE is sensitive to the fraction of aerosols in the fine mode (V_f/V_t), although not to the fine mode effective radius. The intermediate values of AE (≥ 0.5 and ≤ 2.0) can be associated to fine mode fractions in a wide range (0.2–0.85).

Among the Scandinavian and Arctic sites analyzed here (Fig. 8), only Gotland had AE covering a wide range. At this site, AE below 1 is clearly associated to fine mode fractions below 0.5. This is not the case at Andenes, where AE as low as 0.8 had fine mode fractions above 0.5. Conversely, low fine mode fractions (below 0.4) are found at Helsinki and Gotland for AE as large as 1.5. In general the coastal sites exhibit a variable coarse particle contribution that yields to a wider range of fine mode fractions and AE. At the other sites, AE was mainly above 1, and the fine mode fraction of the size distribution ranged from 0.4 to 0.9.

5. Conclusions

Aerosol optical and microphysical properties derived from sunphotometry were analyzed for a number of sites in Scandinavia and Svalbard. The spatial coverage of this kind of data has remarkably improved in the last years, thanks, among other things, to projects within the framework of the International Polar Year 2007–08.

The characterization of the aerosol optical depth revealed different seasonal patterns for the high Arctic, the sub-Arctic region (northern Scandinavia) and Southern Scandinavia. The well-established Arctic haze season followed by a very clean

summer is observed at Svalbard sites. This is not the case over northern Scandinavia, at latitudes about 67–70°N. In that sub-Arctic region, the seasonal pattern is conditioned by the site location and background aerosol, therefore not as uniform as in Svalbard. The arrival of transported aerosols to this area is episodic and not persistent.

In the south, the AOD is higher and the European and Eurasian sources condition the seasonality of aerosol amount and type. The winters are clean, and there are two peaks along the year, one in spring, that coincides with the biomass burning season in Eastern Europe, and the other one in summer. This AOD is associated to high Ångström exponents that qualitatively indicate fine particle predominance.

The aerosol type was analyzed according to previous knowledge of aerosol climatology at key sites. The clean continental, polluted continental and maritime aerosols constitute the three main types, although persistent (Asian) dust was also detected in Svalbard. The average size distributions indicated that, in general, the variations in the fine mode aerosols determine the seasonal variability. The coarse mode aerosol concentrations were very low except for coastal sites.

The inversion of sun/sky radiance data (AERONET sites) allowed characterizing microphysical properties, i.e. the size distribution, volume concentration, fine mode fraction and extinction efficiency. However at most sites the number of data is still too low for a long-term analysis. Furthermore, the low AOD in general does not allow to retrieve information by this method about the absorption characteristics, except in certain episodes, and this information is still missing for an accurate evaluation of the aerosol radiative forcing in the Arctic.

Acknowledgments

Financial support was provided by: the Spanish CICYT (CGL2007-29874-E, CGL2008-05939-C01/CLI, CGL2009-09740 and CGL2010-09480-E); the Norwegian Research Council for POLAR-CAT-Norway; and the Swedish National Space Board and ESA for Norrköping and Palgrunden sites. We thank the AERONET, PHOTONS, RIMA and WRC staff for their scientific and technical support.

References

- Aaltonen, V., Lihavainen, H., Kerminen, V.M., Ginzburg, M., Kulmala, M., Viisanen, Y., 2006. Three years of AOD measurements at three bipolar sites. chapter in NOSA aerosol symposium Helsinki, 2006. Rep. Series Aerosol Science 83, 17–20.
- Alexandrov, M.D., Marshak, A., Cairns, B., Laci, A.A., Carlson, B.E., 2004. Automated cloud screening algorithm for MFRSR data. Geophys. Res. Lett. 31 L04118.
- Ångström, A., 1961. Techniques of determining the turbidity of the atmosphere. Tellus 13, 214–223.
- Bodhaine, B.A., Dutton, E.G., 1993. A long term decrease in Arctic haze at Barrow, Alaska. Geophys. Res. Lett. 20, 947–950.
- Bokoye, A.I., Royer, A., O'Neill, N., McArthur, B., 2002. A North American Arctic aerosol climatology using ground-based sunphotometry. Arctic 55, 215–228.
- Di Pierro, M., Jaeglé, L., Anderson, T.L., 2011. Satellite observations of aerosol transport from East Asia to the Arctic: three case studies. Atmos. Chem. Phys. 5, 2225–2243.
- Dubovik, O., King, M., 2000. A flexible inversion algorithm for retrieval of aerosol optical properties from sun and sky radiance measurements. J. Geophys. Res. 105, 20673–20696.
- Dubovik, O., Smirnov, A., Holben, B.N., King, M.D., Kaufman, Y.J., Eck, T.F., Slutsker, I., 2000. Accuracy assessments of aerosol optical properties retrieved from Aerosol Robotic Network (AERONET) Sun and sky radiance measurements. J. Geophys. Res. 105, 9791–9806.
- Dubovik, O., Sinyuk, A., Lapyonok, T., Holben, B.N., Mishchenko, M., Yang, P., Eck, T.F., Volten, H., Mu noz, O., Veihelmann, B., van der Zande, W.J., Léon, J.F., Sorokin, M., Slutsker, I., 2006. Application of spheroid models to account for aerosol particle nonsphericity in remote sensing of desert dust. J. Geophys. Res. 111 D11208.
- Haywood, J., Boucher, O., 2000. Estimates of the direct and indirect radiative forcing due to tropospheric aerosols: a review. Rev. Geophys. 38, 513–543.

- Herber, A., Thomason, L.W., Gernandt, H., Leiterer, U., Nagel, D., Schulz, K., Kaptur, J., Albrecht, T., Notholt, J., 2002. Continuous day and night aerosol optical depth observations in the Arctic between 1991 and 1999. *J. Geophys. Res.* 107, 4097.
- Holben, B., Eck, T., Slutsker, I., Tanré, D., Buis, J., Setzer, A., Vermote, E., Reagan, J., Kaufman, Y., 1998. AERONET – a federated instrument network and data archive for aerosol characterization. *Remote Sens. Environ.* 66, 1–16.
- Holben, B., Tanre, D., Smirnov, A., Eck, T., Slutsker, I., Abuhassan, N., Newcomb, W., Schafer, J., Chatenet, B., Lavenue, F., Kaufman, Y., Vande Castle, J., Setzer, A., Markham, B., Clark, D., Frouin, R., Halthore, R., Karnieli, A., O'Neill, N., Pietras, C., Pinker, R., Voss, K., Zibordi, G., 2001. An emerging ground-based aerosol climatology: aerosol Optical Depth from AERONET. *J. Geophys. Res.* 106, 12067–12097.
- Kasten, F., Young, A.T., 1989. Revised optical air mass tables and approximation formula. *Appl. Opt.* 28, 4735–4738.
- Korontzi, S., McCarty, J., Loboda, T., Kumar, S., Justice, C., 2006. Global distribution of agricultural fires in croplands from 3 years of Moderate Resolution Imaging Spectroradiometer (MODIS) data. *Glob. Biogeochem. Cycles* 20 GB2021.
- Lund Myhre, C., Toledano, C., Myhre, G., Stebel, K., Yttri, K.E., Aaltonen, V., Johnsrud, M., Frioud, M., Cachorro, V., de Frutos, A., Lihavainen, H., Campbell, J.R., Chaikovskiy, A.P., Shiobara, M., Welton, E.J., Tørseth, K., 2007. Regional aerosol optical properties and radiative impact of the extreme smoke event in the European Arctic in spring 2006. *Atmos. Chem. Phys.* 7, 5899–5915.
- Mazzola, M., Lupi, A., Vitale, V., Tomasi, C., Stone, R.S., Herber, A., Toledano, C., Cachorro, V.E., Torres, B., Berjon, A., Ortiz, J.P., Neill, N.T.O., Masataka, S., Stebel, K., Aaltonen, V., Zielinski, T., Petelski, T., Goloub, P., Blarel, L., Li, Z., Abboud, I., Cuevas, E., Stock, M., Schulz, K.H., Virkkula, A., 2011. Evaluation of Sun photometer capabilities for retrievals of aerosol optical depth at high latitudes: the POLAR-AOD intercomparison campaigns. *Atmos. Environ.*, in press.
- Mitchell, M., 1956. Visual range in the polar regions with particular reference to the Alaskan Arctic. *J. Atmos. Terr. Phys.*, 195–211. Special Supplement.
- Myhre, G., Grini, A., Haywood, J., Stordal, F., Chatenet, B., Tanre, D., Sundet, J., 2003. Modeling the radiative impact of mineral dust during the Saharan Dust Experiment (SHADE) campaign. *J. Geophys. Res.* 108, 8579.
- Myhre, G., Bellouin, N., Berglen, T.F., Bernsten, T.K., Boucher, O., Grini, A., Isaksen, I.S.A., Johnsrud, M., Mishchenko, M.I., Stordal, F., Tanre, D., 2007. Comparison of the radiative properties and direct radiative effect of aerosols from a global aerosol model and remote sensing data over ocean. *Tellus* 59B, 115–129.
- Polissar, A.V., Hopke, P.K., Paatero, P., Kaufmann, Y.J., Hall, D.K., Bodhaine, B.A., Dutton, E.G., Harris, J.M., 1999. The aerosol at Barrow, Alaska: long-term trends and source locations. *Atm. Environ.* 33, 2441–2458.
- Prats, N., Cachorro, V.E., Berjón, A., Toledano, C., de Frutos, A.M., 2011. Column-integrated aerosol microphysical properties from AERONET Sun photometer over Southwestern Spain. *Atmos. Chem. Phys.*, in press.
- Quinn, P.K., Shaw, G., Andrews, E., Dutton, E.G., Ruoho-Airola, T., Gong, S.L., 2007. Arctic haze: current trends and knowledge gaps. *Tellus* 59B, 99–114.
- Quinn, P.K., Bates, T.S., Schulz, K., Shaw, G.E., 2009. Decadal trends in aerosol chemical composition at Barrow, Alaska: 1976–2008. *Atmos. Chem. Phys.* 9, 8883–8888.
- Remer, L.A., Kleidman, R.G., Levy, R.C., Kaufman, Y.J., Tanré, D., Mattoo, S., Martins, J.V., Ichoku, C., Koren, I., Yu, H., Holben, B.N., 2008. Global aerosol climatology from the MODIS satellite sensors. *J. Geophys. Res.* 113 D14S07.
- Rodríguez, E., Frioud, M., Gausa, M., Stebel, K., Mogo, S., Prats, N., Torres, B., Toledano, C., Bastidas, A., Berjon, A., Cachorro, V.E., de Frutos, A.M., 2008. Aerosol optical properties of tropospheric aerosols derived from lidar and Sun photometer measurements at ALOMAR (69°N) in 2005 and 2006. *Optica Pura y Aplicada* 41 (2), 183–190.
- Rodríguez, E., Toledano, C., Cachorro, V.E., Ortiz, P., Stebel, K., Berjón, A., Blindheim, S., Gausa, M., de Frutos, A.M., 2011. Aerosol characterization at the sub-Arctic site Andenes (69°N, 16°E), by the analysis of columnar optical properties. *Q. J. R. Meteorol. Soc.*, in press.
- Schmid, B., Wehrli, C., 1995. Comparison of sunphotometer calibration by Langley technique and standard lamp. *Appl. Opt.* 34, 4500–4512.
- Schuster, G.L., Dubovik, O., Holben, B.N., 2006. Angstrom exponent and bimodal aerosol size distributions. *J. Geophys. Res.* 111 D07207.
- Shaw, G.E., 1983. Sun photometry. *Bull. Am. Meteorol. Soc.* 64, 4–10.
- Shaw, G.E., 1995. The Arctic haze phenomenon. *Bull. Am. Meteorol. Soc.* 76, 2403–2413.
- Sirois, A., Barrie, L.A., 1999. Arctic lower tropospheric aerosol trends and composition at Alert, Canada: 1980–1995. *J. Geophys. Res.* 104, 11599–11618.
- Smimov, A., Holben, B.N., Eck, T.F., Dubovik, O., 2000. Cloud-Screening and quality control algorithms for the AERONET database. *Remote Sens. Environ.* 73, 337–349.
- Solomon, S., Qin, D., Manning, M., Alley, R., Berntsen, T., Bindoff, N., Chen, Z., Chidthaisong, A., Gregory, J., Hegerl, G., Heimann, M., Hewitson, B., Hoskins, B., Joos, F., Jouzel, J., Kattsov, V., Lohmann, U., Matsuno, T., Molina, M., Nicholls, N., Overpeck, J., Raga, G., Ramaswamy, V., Ren, J., Rusticucci, M., Somerville, R., Stocker, T., Whetton, P., Wood, R., Wratt, D., 2007. *Climate Change 2007: The Physical Science Basis*. Cambridge University Press, New York, USA, Chapter Technical Summary Contribution of Working Group 1 to the 4th Assessment Report of the Intergovernmental Panel on Climate Change. pp. 21–87.
- Stohl, A., 2006. Characteristics of atmospheric transport into the Arctic troposphere. *J. Geophys. Res.* 111 D11306.
- Stohl, A., Andrews, E., Burkhardt, J.F., Forster, C., Herber, A., Hoch, S.W., Kowal, D., Lunder, C., Mefford, T., Ogren, J.A., Sharma, S., Spichtinger, N., Stebel, K., Stone, R., Strom, J., Tørseth, K., Wehrli, C., Yttri, K.E., 2006. Pan-Arctic enhancements of light absorbing aerosol concentrations due to North American boreal forest fires during summer 2004. *J. Geophys. Res.* 111 D22214.
- Stohl, A., Berg, T., Burkhardt, J.F., Fjæraa, A.M., Forster, C., Herber, A., Hov, Ø., Lunder, C., McMillan, W.W., Oltmans, S., Shiobara, M., Simpson, D., Solberg, S., Stebel, K., Ström, J., Tørseth, K., Treffeisen, R., Virkkunen, K., Yttri, K.E., 2007. Arctic smoke – record high air pollution levels in the European Arctic due to agricultural fires in Eastern Europe in spring 2006. *Atmos. Chem. Phys.* 7, 511–534.
- Stone, R.S., Anderson, G.P., Andrews, E., Dutton, E.G., Shettle, E.P., Berk, A., 2007. Incursions and radiative impact of Asian dust in northern Alaska. *Geophys. Res. Lett.* 34 L14815.
- Stone, R.S., Anderson, G.P., Shettle, E.P., Andrews, E., Loukachine, K., Dutton, E.G., Schaaf, C., Roman III, M.O., 2008. Radiative impact of boreal smoke in the Arctic: observed and modeled. *J. Geophys. Res.* 113 D14S16.
- Toledano, C., Cachorro, V.E., Berjon, A., Sorribas, M., Vergaz, R., de Frutos, A., Anton, M., Gausa, M., 2006. Aerosol optical depth at ALOMAR observatory (Andoya, Norway) in summer 2002 and 2003. *Tellus* 58B, 218–228.
- Tomasi, C., Vitale, V., Lupi, A., Carmine, C.D., Campanelli, M., Herber, A., Treffeisen, R., Stone, R.S., Andrews, E., Sharma, S., Radionov, V., von Hoyningen-Huene, W., Stebel, K., Hansen, G.H., Myhre, C.L., Wehrli, C., Aaltonen, V., Lihavainen, H., Virkkula, A., Hillamo, R., Stöm, J., Toledano, C., Cachorro, V.E., Ortiz, P., de Frutos, A.M., Blindheim, S., Frioud, M., Gausa, M., Zielinski, T., Petelski, T., Yamanouchi, T., 2007. Aerosols in polar regions: a historical overview based on optical depth and in situ observations. *J. Geophys. Res.* 112 D16205.
- Treffeisen, R., Tunved, P., Ström, J., Herber, A., Bareiss, J., Helbig, A., Stone, R.S., Hoyningen-Huene, W., Krejci, R., Stohl, A., Neuber, R., 2007. Arctic smoke— aerosol characteristics during a record smoke event in the European Arctic and its radiative impact. *Atmos. Chem. Phys.* 7, 3035–3053.
- Waggoner, A.P., Weiss, R., Ahlquist, N., Covert, D., Will, S., Charlson, R., 1981. Optical characteristics of atmospheric aerosols. *Atmos. Environ.* 15, 1891–1909.
- Wehrli, C., 2005. GAW-PFR: a network of aerosol optical depth observations with precision filter radiometers. In: *WMO/GAW Experts Workshop on a Global Surface Based Network for Long Term Observations of Column Aerosol Optical Properties Technical Report*. GAW Report No. 162, WMO TD No. 1287.
- WMO, 2005. *WMO/GAW Experts Workshop on a global surface-based network for long term observations of column aerosol optical properties*. WMO TD No. 1287, Davos, Switzerland, 8–10 March 2004, 153 pp.
- Zdun, A., Rozwadowska, A., Kratzer, S., 2011. Seasonal variability in the optical properties of Baltic aerosols. *Oceanologia* 53, 7–34.